

MMA Memo 211

Accurate Amplitude and Flux Calibration of the MMA

M. S. Yun, J. Mangum, T. Bastian, M. Holdaway
National Radio Astronomy Observatory

J. Welch
University of California, Berkeley

May 15, 1998

Abstract

The 10% amplitude calibration accuracy achievable with the current standard calibration techniques may be sufficient to produce images with dynamic range of $\leq 10^3$, but achieving a dynamic range of 10^4 or higher with the MMA requires better than 1 percent accuracy in amplitude calibration. A self-calibration technique may be applied to improve images, but it may not be possible in all cases. Therefore, an emphasis is given to achieving accurate initial calibration. Multi-transition spectroscopic studies and multi-array synthesis also require high accuracy in absolute sense as well.

The conventional “chopper wheel” and a two temperature load method for amplitude and flux calibrations are examined. The two temperature load calibration offers a potential to achieve the 1% accuracy in amplitude and flux calibration, but it is technically challenging. In comparison, the chopper wheel gain calibration and astronomical flux calibration cannot provide better than 5% accuracy. Whether the more complex two temperature load system is justifiable for the MMA may ultimately dependent on how well the radiometric phase correction will work. Several other relevant issues including establishment of astronomical flux standards are discussed, and engineering goals are identified.

1 Introduction

The aim of amplitude and flux calibration is to convert the output voltage or counts from the correlator into brightness temperature or flux density by carefully tracking the instrumental and atmospheric variations and determining accurate conversion factors. Because the adverse effects of instrumental and atmospheric variations grow rapidly with frequency, standard calibration procedures will not work well at submillimeter wavelengths. The high design goals of the MMA (e.g. high sensitivity and imaging with large dynamic range) also demand a much higher calibration accuracy than achieved by the conventional technique used at the existing millimeter arrays (about 10%).

In this memo, we first evaluate the required amplitude calibration accuracy in terms of the effects of amplitude error on the dynamic range of the images produced. In the following sections, the conventional “chopper wheel” calibration method and a two temperature load calibration method are described. In §4, several potential approaches for flux calibration using astronomical sources and a direct calibration using the two temperature load system are considered. Flux calibration is discussed here in conjunction with amplitude calibration to bring attention to the fact that large amplitude gain variations expected at mm and submm wavelengths make the flux calibration inseparable from gain calibration. Additionally, the two temperature load calibration scheme can potentially offer the 1% accuracy needed in both amplitude and flux calibration simultaneously. Some special concerns for the MMA calibration such as polarization and solar observations are addressed and several engineering goals are identified in §5 and §6. Pointing error is another contributor to the gain drift, but it is already addressed extensively in the context of a more stringent requirement for mosaic imaging by Holdaway (1997b).

2 How Accurate Should the Calibration Be?

The dynamic range (DR) achievable from an observation of length τ , calibrated at interval t using an interferometer array with N antennas is

$$DR = \sqrt{M \times N(N-1)}/\sigma_\phi = \sqrt{M \times N(N-1)}/\sigma_A \quad (1)$$

where $M = \tau/t$ is the number of samplings of the atmosphere, and σ_ϕ and σ_A are random Gaussian errors in phase and amplitude (Perley 1989). As

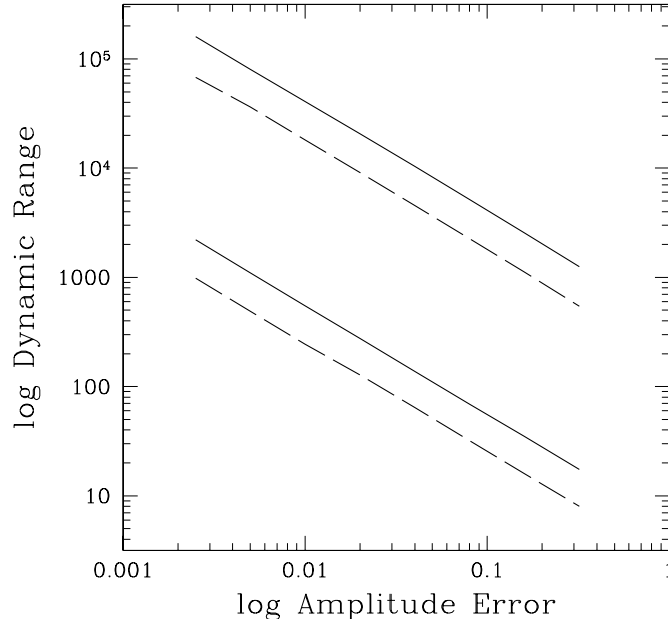


Figure 1: Plot of dynamic range achievable as a function of amplitude error. The dynamic ranges are determined from the simulated observations of a single point source at the phase center using a 40 element array with a 20 minute duration. For the upper pair of the lines, antenna based Gaussian amplitude gain error are assumed with a calibration intervals of 40 seconds (solid line) and 200 seconds (broken line). The lower pair corresponds to the compact array case where the amplitude fluctuations are 100% correlated among the antennas.

pointed out by Perley, an important consequence of Eq. 1 is that “a 10° phase error is as bad as 20% amplitude error”. Therefore, the dynamic ranges achievable with the MMA in most cases – particularly at high frequencies – will critically depend on accurate radiometric and astronomical phase calibration.

Self-calibration (Cornwell & Fomalont 1989) can be used to improve dynamic range if the source visibility is well determined with high S/N so that both M and $\sigma_\phi(\sigma_A)$ can be improved using the on-source data. While the phase self-calibration is relatively easy to achieve, amplitude self-calibration generally demands a higher S/N so that achieving high accuracy in the

initial amplitude calibration is highly desirable. Using an idealistic assumption that no phase error exists, the effect of amplitude error on the achieved dynamic range can be estimated from a set of simulated observations (see Figure 1). The results agree well with the estimates using Eq. 1, and we find that a modest dynamic range of $DR \sim 10^3$ can be achieved even with 10% amplitude error. On the other hand, achieving a dynamic range better than 10^4 may require an amplitude calibration accuracy of 1% or better.

For a compact configuration where the amplitude fluctuation due to atmosphere is correlated among the antennas, Eq. 1 is no longer valid. In the extreme case of 100% correlated fluctuations, the benefit of having N independent samples goes away, and the dynamic range is given by

$$DR = \sqrt{M}/\sigma_A \quad (2)$$

Therefore, achieving high dynamic range requires *more frequent amplitude calibration* than in larger configurations. A more realistic scenario must lie between the two extreme cases considered (two sets of lines in Figure 1), and better than 5% calibration accuracy is needed to achieve a dynamic range of 10^3 and better than 1% accuracy for $DR \geq 10^4$. In all cases, minimizing error in each calibration measurements is essential in achieving high dynamic range.

3 Amplitude Calibration

3.1 Single Load Calibration (“Chopper Wheel” Method)

The conventional amplitude calibration methods used by existing millimeter arrays are similar to the methods used at lower frequencies (e.g. the VLA) with a few important exceptions. The overall gain variation is measured and corrected by frequent observations of a nearby calibrator assuming the system and the atmosphere are stable over several minutes and over ~ 10 degree separation in the sky.

A major additional concern at mm and submm wavelengths is the contribution to the noise (or gain) by the atmosphere. The amplitude gain calibration is in essence the tracking of system (noise) temperature

$$T_{sys} = \frac{e^\tau}{\eta_l \eta_{fss}} [T_{rec} + T_{sky} + T_{ant} + T_{cmba}] \quad (3)$$

where

- $\eta_l = \eta_r \eta_{rss}$ is antenna efficiency including ohmic losses and rearward spillover and scattering,
- η_{fss} is forward spillover and scatter efficiency,
- T_{rec} is receiver noise temperature,
- $T_{sky} = \eta_l(1 - e^{-\tau})T_{atmo}$ is noise due to the atmosphere,
- $T_{ant} = (1 - \eta_l)T_{spill}$ is noise from the antenna,
- $T_{cmba} = \eta_l e^{-\tau} T_{CMB}$ is noise from the cosmic microwave background.

The atmospheric opacity τ is used to compute the effective gain above the atmosphere so that as $\tau \rightarrow \infty$, $T_{sys} \rightarrow \infty$ (no sensitivity). In practice, T_{sys} is determined by comparing the receiver output power from an ambient temperature load with that of the sky (see Kutner & Ulich 1981)

$$T_{sys} = \left(\frac{T_{load} - T_{sky}}{P_{load} - P_{sky}} \right) P_{sky} - T_{sky} \quad (4)$$

where P_{sky} and P_{load} are measured power on the sky and on the load, and T_{sky} is estimated from antenna efficiency and an atmospheric model. T_{sys} is measured frequently (e.g. every 5 minutes) to calibrate the atmosphere, and the effects of varying opacity, both in time and in elevation, are then removed from the measured fringe amplitude by

$$F(Jy) = constant \times T_{sys} \times f(volts). \quad (5)$$

The main advantage of the chopper wheel method is its simplicity (see Eq. 4). Even in the worst case scenario, one can achieve a dynamic range of 100 or better (see Fig. 1), and this is the reason why it is successfully used with all existing millimeter arrays. The main disadvantage is that it has an internal consistency of only about 10% because T_{sky} and T_{load} are not well determined and varying in time. At millimeter and submillimeter wavelengths, the atmosphere contributes significantly to the T_{sys} , but T_{sky} (in Kelvin) and atmospheric opacity estimated from weather data and an atmospheric model are only accurate to 5-10%. The median opacity at 450, 650, and 850 GHz are expected to be about unity at the Chajnantor site, and tracking amplitude gain using an ambient load (Eq. 4) may pose a sensitivity problem.

3.2 Two Temperature Load Calibration

Achieving a more accurate amplitude calibration may require computing T_{sys} directly from Eq. 3 by determining each of the individual noise terms explicitly. First, all antenna terms (η_l , η_{fss} , T_{ant}) should be measured and tracked. Even for the chopper wheel calibration, the antenna efficiencies, which are usually assumed to be constant but may vary significantly with temperature and elevation, need to be tracked for an improved calibration. Frequent monitoring of antenna efficiencies using a nearby transmitter and holography as well as structural analysis may be highly desirable for optimum operations at high frequencies anyhow, and blockage, scattering, and sidelobe responses of the antennas should be well understood in the first place as part of the antenna design study. The efficiencies of the BIMA antennas were measured in the early 80's at 1 cm wavelengths with about 4% accuracy. The new MMA antennas with strong emphasis on the design should be better understood and measured more accurately. [A case for a smaller diameter antenna design may be made here if understanding the antenna gain responses at high frequencies become the ultimate limit in achieving high calibration accuracy.]

Determining T_{sky} requires measuring both τ and T_{atmo} . The atmospheric opacity τ at the observing frequency can be obtained either directly by antenna tipping or indirectly from radiometry (see Carilli et al. 1998). In principle the radiometric measurements can be used to infer the opacity at the observed frequency, but the current atmospheric model is inadequate to transfer a radiometric measurement from one frequency to another with 1% accuracy. Direct measurement by tipping is more accurate as long as the receiver system is stable, and it is favored at the moment. One or more antennas may be dedicated to continuous monitoring of opacity at the observed frequency (see calibration subarray discussion in §5.2). Determining T_{atmo} still requires an atmospheric model, but the error in T_{atmo} (typically $\sim 10\text{K}$) is not as critical as in the ‘‘chopper wheel’’ case because its contribution to the overall error is reduced by a factor τ [$T_{sky} \approx (1 - e^{-\tau})T_{atmo} \approx \tau * T_{atmo}$ for $\tau \ll 1$].

Accurate measurement of T_{rec} can be achieved if well calibrated loads at two different temperature are used and the receiver response is linear. The output power from the receiver is given by:

$$P = K \times T_{in} + P_0 \tag{6}$$

where $T_{in} = T_{rec} + T_{ant} + T_{sky} + T_{load}$. The coefficient K can be determined

directly from having two different temperature loads,

$$K = \frac{P_2 - P_1}{T_2 - T_1} \quad (7)$$

where T and P are the effective load temperature and measured output power. The constant offset P_0 can be measured by turning off the amplifier on the detector, and now T_{rec} (and thus T_{sys}) can be computed.

Bock et al. (1998) have considered a two temperature load system for the BIMA array that uses a rotating mirror assembly located behind the subreflector and tabs the two temperature controlled loads with about 2% coupling. The small central area in the subreflector normally reflects the ambient radiation from the room behind the vertex window back into the Cassagrain feed, and if not scattered away, this can introduce significant additional noise. In place of putting a scatter cone, a small hole just the image of the vertex window is made in the center of the secondary and a rotating mirror system is placed so that the hole is effectively filled with (a) a 300 K load, (b) a 400 K load, or (c) a scattering mirror which functions the same way as the scattering cone. For $BW = 8$ GHz and $T_{sys} = 50$ K, the continuum sensitivity of the MMA, σ_T , is about 0.0006 K with 1 second integration, and the ΔT_{cal} of 6-8 K can be measured with $S/N \geq 10^4$. Unlike the chopper wheel case where the ambient load can saturate the detector, the resulting load is much closer to the signal from astronomical sources and operates within the same linear regime of the detectors.

Among the terms contributing to T_{sys} in Eq. 3, the antenna and the CMB terms are expected to be varying slowly over time, and only T_{rec} and T_{sky} terms may vary on short time scales. The 225 GHz opacity and 11.2 GHz phase stability data at Chajnantor and atmospheric transmission models suggest that the amplitude fluctuations over short time scales (10-30 seconds) will typically be well below 1% level at 345 GHz, rising to a few percent at 650 GHz (Holdaway 1998a). Therefore, the T_{sky} term also has a minor contribution to amplitude gain fluctuation except at the highest frequencies. The quantitative understanding of the stability of the receiver system (T_{rec}) has not been demonstrated yet, but the two temperature load system with a rotating mirror provides both the means to measure the receiver temperature and its stability and also possibly a way to track and remove its effects (by observing with the spinning mirror system continuously on) so that the 1% relative calibration accuracy can be achieved. If all antenna terms are accurately known, achieving an absolute calibration at 1% accuracy level in total system gain may be possible. An important

additional benefit is that it automatically provides absolute flux calibration of the system without resorting to any astronomical source (see below). It can also be used to inject a well calibrated signal to test and calibrate the entire system. For example, a one MHz spectral channel can be calibrated to 1% accuracy with a 10 second integration.

4 Flux Calibration

4.1 Direct Instrumental Calibration

For a well calibrated system where all the gain terms are measured and tracked, a direct conversion from measured counts in total power and interferometric modes can be translated directly into flux units so that many difficulties associated with the astronomical calibration (see below) will disappear. The effective radiation temperature T_R of a source with excitation temperature T_{ex} and optical depth τ_ν is given by

$$T_R = (1 - e^{-\tau_\nu})[J(\nu, T_{ex}) - J(\nu, T_{CMB})] \quad (8)$$

where $J(\nu, T) = (h\nu/k)/[\exp(h\nu/kT) - 1]$, h and k are Planck's constant and Boltzmann's constant, and T_{CMB} is the microwave background temperature. The observed source antenna temperature T_A for a normalized source brightness distribution $B_n(\Psi)$ in the direction of Ω on the sky is then

$$T_A = T_R \eta_r \left[\frac{\int \int_{\Omega_s} P_n(\Psi - \Omega) B_n(\Psi) d\Psi}{\int \int_{4\pi} P_n(\Omega) d\Omega} \right] e^{-\tau} \quad (9)$$

where P_n is the normalized antenna power pattern ($P_n(0) = 1$), and Ω_s is the solid angle subtended by the source (see Eq. 3 of Kutner & Ulich 1981). In general, the source distribution is not known *a priori*, and the corrected radiation temperature $T_R^* \equiv \eta_c T_R$ is commonly used because it is a source and telescope independent quantity and a good estimate of T_R as the source coupling factor $\eta_c \sim 1$ in most cases. One can further show that the source antenna temperature corrected for atmospheric attenuation $T'_A \equiv e^\tau T_A$ is related to T_R^* as

$$T'_A = T_R^* \eta_l \eta_{fss} \quad (10)$$

If the antenna temperature is measured as a function of airmass with antenna tipping, η_l can be determined along with τ . (The corrected antenna temperature T_A^* is related to T_R^* by the relation $T_A^* \equiv T'_A / \eta_l = \eta_{fss} T_R^*$.)

One of the important advantages of the two temperature load calibration scheme (§3.2) is that it requires knowing and tracking all antenna efficiency terms needed for a direct flux conversion. Both the VLA and VLBA uses an internal calibration signal, “ T_{CAL} ”, and estimated antenna gains to achieve good relative calibration, and an astronomical source is used to set the flux scaling. The two load calibration system provides an extremely accurate T_{CAL} signal, which can be used directly to convert the measured power directly to flux density (Jy). Since T_R^* is independent of observed telescope, the accuracy of the method can be checked by comparing with measurements made at other telescopes or by examining with a detailed model of Mars (see below).

4.2 Flux Calibration using Astronomical Sources

The conventional flux calibration scheme with existing telescopes is to track the relative instrumental gains and determine the flux scaling using “known” astronomical standards, whose fluxes are tied to a small number of careful measurements using a well calibrated horn or a small antenna. Even if the MMA adopts the two temperature load system for flux and gain calibration, establishing a set of astronomical flux standards will be necessary for calibration verification. In the event that the antenna terms are not easily measured or tracked to the needed accuracy, observations of astronomical calibrators may be used to determine the antenna gain terms.

A good astronomical flux calibrator has the following properties: (1) unresolved size; (2) constant or theoretically predictable flux; and (3) bright. At millimeter and submillimeter wavelengths, few if any sources meet all of these criteria. The current generation millimeter interferometers calibrate flux using variants of the following procedure (also see MMA Memo 149 by Holdaway 1996):

- Observe a planet with some or all antennas in total power mode to set the total power flux scale. The planet is the “primary flux calibrator”.
- Observe a bright quasar with some or all antennas in total power mode to determine the quasar flux. The quasar is the “secondary flux calibrator”.
- Observe the same bright quasar, now of known flux, with all antennas in interferometric mode to set the interferometric flux scale.

- Correct these observations for elevation-dependent antenna and atmospheric effects such as the gain curves and time dependent atmospheric attenuation.

This calibration system is an extension of the flux calibration system used with millimeter and submillimeter single dishes. The key step in this calibration scheme is the determination of the flux of the primary calibrator (the planets). We discuss below potential uses of various astronomical objects for flux calibration of the MMA.

Moon. Because of its large size compared with the primary beam of the MMA, the limb of the moon offers essentially a one-dimensional knife edge, the Fourier transform of which is

$$F(\omega) = T_{\circ}[\pi\delta(\omega) - i\frac{1}{\omega}] \quad (11)$$

where T_{\circ} is the temperature of the moon. The real part of the Fourier transform is a delta function, but there is also an imaginary component that decreases as $1/\omega$. While this offers an interesting application in the interferometric mode, T_{\circ} is a poorly determined quantity and has a well known dependence on the details of the surface features. Given these uncertainties, flux calibration using the limb of the moon is expected to be less reliable than using the planets.

Planets. Nearly all flux scaling for commonly used flux standards at millimeter and submillimeter wavelengths are based on measurements of planets (see Ulich 1974, Ulich et al. 1980, also Muhleman & Berge 1991). The planets for which the brightness temperatures are best known in the millimeter and submillimeter range are Mars and Jupiter, with Mars probably best understood. Unfortunately, these two planets are heavily resolved by the MMA, particularly at the higher frequencies. This may not be as much of a problem if accurate single dish total power measurements are available for the MMA antennas, however. In any case, the brightness temperatures (and their distribution across the visible disk) for these bodies are not as precisely known as desired.

For Mars, the whole-disk brightness temperatures predicted at millimeter and submillimeter wavelengths by the best current models are probably only good to 10-20%. This is due to uncertainties in regolith dielectric and roughness properties, and uncertainties in ice cap thermal properties (both the residual H₂O and the seasonal CO₂ caps). Interferometric observations of Mars by the fully functional MMA will help constraining some of these

uncertainties (e.g., the polarized flux density can be used to help constrain the dielectric and roughness properties), so when the MMA has matured to some degree, this situation should improve considerably. In addition to these uncertainties, there may be unmodeled temporal variations due to local and global dust storms, which may affect the flux density at the shortest wavelengths. These storms can be tracked through monitoring of the CO line, and some care should be taken. Modeling gaseous giant planets is much harder as their continuum spectra are not well understood.

Asteroids. Asteroids are compact and bright blackbody emitters and thus potentially promising primary flux calibrators. The bolometer observations at 250 GHz of 15 nearby asteroids (heliocentric distance $r = 2.0$ -3.5 au, geocentric distances $\Delta = 1$ -5 au) by Altenhoff et al. (1994) found strong continuum emission (50-1200 mJy; $T_B = 150$ -200 K), which agrees with the blackbody model within the uncertainty of calibration on Mars. They are compact, $\theta_D(\prime\prime) = 0.28 [D/(200 \text{ km})][r(\text{pc})]^{-1}$ – an order of magnitude smaller than Uranus or Neptune. Their flux density changes significantly due to their and Earth’s orbital motion around the Sun, but the changes are highly predictable. Because they are not perfectly round, small oscillation in observed flux is also expected from their rotation – about 4% peak to peak over 9 hour period for Ceres (Altenhoff et al. 1996).

As is the case for the VLBA, the high spatial resolution achievable with the MMA presents a fundamental problem in that most of these “primary” flux calibrators are highly resolved at the maximum resolution of the array – for example, the 3 km baseline corresponds to $8.5 \times 10^6 \lambda$ at 850 GHz or an angular resolution of 24 mas. The thermal emission from the photosphere in the nearby stars offer an interesting possibility for MMA flux calibration.

Main Sequence Stars. The Sun at a distance of 10 pc is about 1 mas in diameter and will have about 1.3 mJy of thermal continuum flux at 650 GHz. Active regions on the Sun will cause some flux variations, perhaps at the few percent level or less. The zodiacal dust in the solar system may be at the level of 1 percent or more, depending on how much cool dust resides in the outer parts of the solar system. Predicting the precise flux (likely to be somewhat higher because of the higher effective temperature at mm wavelengths) will require fairly detailed models of stellar atmospheres.

By searching the HIPPARCOS data set, Richard Simon has found that there are 250 stars which will be brighter than 2 mJy at 650 GHz. The number of non-variable, non-binary, main-sequence stars visible from Chajnantor is much smaller – 22 stars, listed in Table 1. There are probably other suitable stars which are not listed as main sequence. The integration times

needed to achieve SNR=20 are about 10 minutes in most cases, computed assuming an rms noise of $0.50 * [t(\text{min})]^{-1/2}$ mJy (sensitivity for a 40×10 -m array, corrected for the collecting area from the sensitivity calculation by Holdaway 1997a).

Giant and Supergiant Stars. While G, K, and M giant and supergiant stars are cooler on average compared to the main sequence stars, they are generally larger and thus brighter at longer wavelengths. We have searched the Bright Star Catalog (Hoffleit 1982) for all giant and supergiant stars with V band magnitude smaller than 5. After excluding all binaries and variables, stars with estimated and measured diameters published by Ochsenbein & Halbwachs (1982) are tabulated in Table 2. Using the effective temperature taken from Allen (1973), the 650 GHz fluxes are estimated assuming thermal emission from a face-on stellar disk ($S_\nu = 2kT\nu^2\Omega/c^2$). On average, these stars are nearly 10 times brighter at submillimeter wavelengths than the main sequence stars in Table 1 so that SNR=20 detection can be achieved in less than a minute in most cases. Some of these may still turn out to be variable, but the MMA can establish this quickly and accurately with a modest monitoring program. This list is only partially complete as stellar diameters are available only for a subset of our original list.

Compact Galactic thermal sources such as ultra-compact HII regions such as W3(OH) or stellar sources such as CRL618 and IRC+10216 are commonly used secondary flux standards used by existing submillimeter telescopes such as CSO and JCMT. These objects are typically 5-10'' in size and have observed fluxes of 1-10 Jy at 230 GHz and 20-200 Jy at 650 GHz (see Sandell 1994). These objects may be used for flux calibration by the MMA in the total power mode (in place of the planets when they are not available), but they are not likely to be useful in the interferometric mode because of their large sizes and complex structures.

Lastly, one serious concern for astronomical flux calibration of the MMA is accurate bootstrapping of the flux scaling from the primary calibrator to the secondary or gain calibrators if they are observed hours apart in time. An accurate accounting of the temporal gain variation should be applied before any flux scale factors are applied. For tracks covering only a small range of hour angle (e.g. shadowing, transit at low elevations, snapshot imaging – see Holdaway 1998b), observing a primary flux calibrator at the same elevation range as the gain calibrator and the program sources may not always be possible.

5 Special Considerations for the MMA Calibration

5.1 Amplitude Decorrelation

Atmospheric phase fluctuations and resulting amplitude decorrelation are serious concerns for the MMA operating at higher frequencies as the amplitude loss scales as $e^{-\sigma_\phi^2/2}$ and the rms phase error σ_ϕ increases linearly with frequency (see MMA Memo 136, Holdaway & Owen 1995 and references therein). The amplitude loss due to rms phase fluctuations of 30° and 70° are 13% and 50%, respectively, with corresponding effective losses in sensitivity. The affected fraction of time due to atmospheric phase fluctuations and expected loss of sensitivity as function of frequency are shown in Table 3. Fortunately the short integration time required for the phase calibration (see Holdaway & Owen 1995, Rupen 1997) will simultaneously address the amplitude decorrelation problem as the phase coherent time scale for the array at the highest frequency is still several seconds long. The radiometric phase correction may further increase the coherence time by a factor of 3 to 4.

5.2 Dedicated Calibration Subarray

Can the radiometric opacity measurements be successfully transferred to the observed frequency with better than a few percent accuracy needed? The analysis of the radiometric measurements for the MMA by Carilli, Lay, & Sutton (1998) suggests that absolute calibration of the radiometer may not be adequate for a reliable estimation of opacity at other frequencies, primarily because of the shortcomings in the atmospheric model.

Alternatively one or more antennas may be dedicated to monitoring opacity of the atmosphere at the exact observing frequency. The double load calibration and direct flux calibration relies on accurate knowledge of opacity at the observed frequency. There may be other beneficial uses of a dedicated calibration subarray such as the calibration of the radiometric system as discussed by Carilli et al. (1998).

5.3 Short Tracks

A large fraction of MMA tracks may be too short in duration to derive the elevation-dependent gain or to obtain its own flux and opacity data

(see Holdaway 1998b). Since the primary observing mode of the MMA is service observing so that only the final calibrated data are delivered to the proposers, some of the calibration may be done in a less traditional way. For example, instrumental gain terms such as antenna deformation, spillover and scatter, and ground pick-up may be corrected using an analytic model or a look-up table, disjointed from the temporal changes due to the receiver gain and atmospheric variations. Also a good database of secondary flux calibrators (quasars, stars – see §4.2) may be maintained and utilized rather than requiring an observation of a primary calibrator in each track. A direct calibration approach using model antenna gains and temperature calibrated loads (§4.1) offers many attractive aspects.

5.4 Polarization Observations

Measuring polarized continuum and spectral line emission is one of the important scientific goals for the MMA. Linear polarizer is commonly used by existing millimeter arrays for its simplicity, but linear polarizers can complicate the flux and amplitude calibration as many quasars (gain and secondary flux calibrators) are intrinsically polarized (a few to 10%). The amplitude variation as a function of parallactic angle due to polarized emission is confused with instrumental gain variation unless the intrinsic polarization of the calibrator is known and accounted for. Polarized flux may also be time variable. Therefore, the degree of polarized emission should be included as an additional consideration for MMA calibrators. Alternatively, circular polarization scheme may be considered instead.

5.5 Solar Observations

Modern radio telescopes are designed to observe sidereal sources with the best sensitivity that present-day technology allows. This means minimizing T_{sys} by designing low-noise receivers, minimizing antenna spillover, blockage, etc. These efforts are for naught when observing the Sun. The Sun is much bigger and brighter than any other source in the sky at all frequencies above 100 MHz. Consequently, the contribution to T_{sys} by the Sun dominates all others, usually by a wide margin. For example, at a wavelength of 20 cm, T_{ant} is roughly 50,000 K, far greater than the 35 K T_{sys} one normally encounters. At the VLA, the gain is reduced by using 20 dB, phase-constant, switched attenuators. T_{sys} is measured with the attenuators in place by means of high amplitude T_{cal} . These two modifications enable one to phase-

calibrate the array in the normal way (by referencing the observations to a phase calibrator source), and to flux calibrate by referencing the signal to the high T_{cal} .

The MMA will face similar problems. T_{ant} will be about 4800 K for quiet Sun conditions at a wavelength of 1 mm. Again, this is much larger than the system temperatures anticipated. The solar signal must therefore be attenuated by 15-20 dB. With the attenuation in place, one cannot observe a calibrator. Hence, the attenuation must be switched out of the signal path when observing a calibrator source. How will gain reduction be achieved at the MMA? Through one or more fixed attenuators? Or the use of automatic gain control with a large dynamic range? In either case, we must be able to accurately measure and correct for the gain change and possible phase shifts introduced by fixed attenuators or AGC. In AGC is employed, it must operate on a time constant less than that of possible transient activity ($\ll 1$ second). And, like the VLA, it is likely that a known T_{cal} signal will need to be injected. A possible option for monitoring gain and phase variations is the use of a pulse cal, as used to some extent in the VLBA (at least at low frequencies).

If the solution lies in AGC, we need to know how much dynamic range is needed. For quiet Sun observations, the AGC would need to insert 15-20 dB of additional attenuation. And for solar bursts, an additional 20 dB of attenuation may be needed, for a total of 35-40 dB over and above the normal operating point of the ALC.

6 Summary and Engineering Concerns

We have examined the flux and amplitude gain calibration requirements for the MMA. The standard calibration techniques are compared with the two temperature load calibration system. Special topics relevant for the MMA are also considered. The conclusions are:

1. The standard calibration techniques routinely used by the current generation of millimeter interferometers are good enough to provide dynamic ranges of 10^2 to 10^3 , but a more accurate technique is needed to achieve a dynamic range better than 10^3 , especially for the compact configurations where the amplitude fluctuation is correlated for the entire array. It should also be noted that the dynamic range is limited more severely by the phase error (Eq. 1) – “a 10° phase error is as bad as 20% amplitude error” (Perley 1898).

2. The conventional “chopper wheel” method of gain calibration is simple and sufficiently accurate for the current millimeter arrays. However, it is reliable to only about 10% accuracy because of large errors in T_{sky} and T_{load} . High opacity in the high frequency windows of the MMA may also pose a problem.

3. A strong case may be made for a two temperature load calibration scheme such as proposed by Bock et al. (1998). By tracking the individual components of T_{sys} (Eq. 3) explicitly to 1% accuracy level, both absolute and relative gain calibration of 1% accuracy may be achievable. An extensive bookkeeping of parameters such as antenna gains and atmospheric opacity is needed to a high accuracy, but such an effort is necessary to achieve high dynamic range ($> 10^3$). In addition, such a system also offers a capability for direct flux calibration and internal calibrations (e.g. bandpass measurements).

4. A need for establishing astronomical flux calibrators exists in any event, and several potential calibrators are examined. The thermal emission from giant and supergiant stars offers many attractive features such as high brightness and compactness (≤ 10 mas). Planets such as Mars and asteroids are also highly promising. In all cases, some additional work such as flux monitoring or modeling is needed to improve calibration reliability.

5. Some special considerations such as amplitude decorrelation, use of calibration subarray and dedicated calibration runs, polarization observations, and solar observations are also briefly discussed.

Lastly, the engineering issues identified for achieving highly accurate amplitude and flux calibration and special observations include:

- All antenna efficiencies such as ohmic loss, forward and rearward spillover, and scatter, should be measured accurately (good to 1% level). The beam patterns and aperture efficiency of the individual antennas should be mapped and optimized using holography. Establishing a good understanding of time and elevation dependent changes such as dish deformation or ground pick-up (via a model or look-up tables) would greatly benefit instrument-based calibration schemes.
- Receiver stability may be the dominant contributor to the short term amplitude variation. Achieving high stability or employing a means to track receiver gain variability such as the two temperature load system are highly desirable.

- LO coherence has been identified as a potentially important source of phase error and receiver system stability, particularly at high frequencies.
- Selection of instrumentation for polarization measurement needs to take into account the potential difficulties associated with gain calibration. If linear polarizers are adopted, then extra care should be given to intrinsically polarized emission from the calibrators.
- A workable scheme for the use of attenuators and ALC for the solar observations needs to be worked out. A special source of T_{cal} signal may also be needed.

Table 1: Candidate main sequence stars for primary flux calibration.

Catalog No.	Name	RA (B1950)	Dec (B1950)	Parallax (")	V (mag)	Spec Type	T_{eff} (K)	Diam. (mas)	S_{650} (mJy)	t_{int}^{\dagger} (min)
113368	24Alp PsA	343.73	-29.89	0.130	1.17	A3	8720	2.2	11.8	0.7
7588	Alp Eri	23.97	-57.49	0.023	0.45	B3	18700	1.5	7.9	1.6
8102	52Tau Cet	25.42	-16.19	0.274	3.49	G8	5570	2.1	5.1	3.8
49669	32Alp Leo	151.43	12.21	0.042	1.36	B7	13000	1.4	5.0	4.0
108870	Eps Ind	329.97	-57.02	0.276	4.69	K5	4350	2.3	4.9	4.2
66459		203.81	35.97	0.092	9.06	M9	2500	5.3	4.3	5.4
22449	1Pi 3Ori	71.79	6.88	0.125	3.19	F6	6360	1.6	4.2	5.7
9236	Alp Hyi	29.31	-61.81	0.046	2.86	F0	7200	1.5	4.0	6.3
54872	68Del Leo	167.87	20.80	0.057	2.56	A4	8460	1.3	3.5	8.2
8903	6Bet Ari	27.97	20.56	0.055	2.64	A5	8200	1.3	3.5	8.2
57757	5Bet Vir	177.03	2.05	0.092	3.59	F8	6200	1.5	3.2	9.8
71908	Alp Cir	219.60	-64.76	0.061	3.18	F1	7045	1.3	3.1	10.4
84143	Eta Sco	257.14	-43.18	0.046	3.32	F3	6740	1.4	3.1	10.4
19849	40Omi2Eri	63.22	-7.77	0.198	4.43	K1	5080	1.6	3.1	10.4
27072	13Gam Lep	85.59	-22.47	0.111	3.59	F7	6280	1.4	3.0	11.1
65109	Iot Cen	199.44	-36.45	0.056	2.75	A2	8970	1.0	2.6	14.8
15510		49.53	-43.25	0.165	4.26	G8	5570	1.5	2.5	16.0
109176	24Iot Peg	331.18	25.10	0.085	3.77	F5	6440	1.2	2.4	17.4
78072	41Gam Ser	238.54	15.81	0.090	3.85	F6	6360	1.2	2.3	18.9
69701	99Iot Vir	213.35	-5.77	0.047	4.07	F7	6280	1.1	2.0	25.0
64394	43Bet Com	197.38	28.14	0.109	4.23	G0	6030	1.2	1.9	27.7
28103	16Eta Lep	88.53	-14.17	0.066	3.71	F1	7045	1.0	1.9	27.7

\dagger Required integration time to achieve SNR=20 assuming rms sensitivity of $0.50*[t(min)]^{-1/2}$ mJy.

Table 1. A list of 22 bright main sequence stars visible from Chajnantor that are non-variable and non-binary with expected 650 GHz flux ≥ 2 mJy, compiled by Richard Simon. They are unresolved by the 3 km baseline of the MMA, and the thermal blackbody emission from the 5 brightest stars can be detectable with SNR=20 in 5 minutes of integration.

Table 2: Candidate giant and supergiant stars for primary flux calibration.

HD No. No.	Name	RA (J2000)	Dec (J2000)	Parallax (")	V (mag)	Spec Type	T_{eff} (K)	Diam. (mas)	S_{650} (mJy)	t_{int}^{\dagger} (sec)
3627	31Del And	01:39	+30:51	0.028	3.27	K3 III	4000	4.6	19.	17
12274	59Ups Cet	02:00	-21:04	0.007	4.00	M0 III	3200	6.4	31.	6.2
24512	Gam Hyi	03:47	-74:14	0.005	3.24	M2 III	3000	9.8	67.	1.3
25422	Del Ret	03:58	-61:24	-0.001	4.56	M2 III	3000	4.6	15.	27
28028	43 Eri	04:24	-34:01	-0.008	3.96	K4 III	3900	4.8	21.	14
39425	Bet Col	05:50	-35:46	0.023	3.12	K2 III	4300	4.1	17.	21
45348	Alp Car	06:23	-52:41	0.028	-0.7	F0 II	7100	6.5	70.	1.2
50310	Tau Pup	06:49	-50:36	0.007	2.93	K1 III	4400	4.4	20.	15
50778	14The CMa	06:54	-12:02	0.022	4.07	K4 III	3900	4.1	15.	27
63700	7Xi Pup	07:49	-24:51	0.003	3.34	G6 I	4800	3.9	17.	21
76294	16Zet Hya	08:55	+05:56	0.035	3.11	G9 II	4400	3.5	13.	36
82150	Eps Ant	09:29	-35:57	0.005	4.51	K3 III	4000	4.3	17.	21
87835	31 Leo	10:07	+09:59	0.000	4.37	K3.5 III	3600	3.3	9.1	72
90432	42Mu Hya	10:26	-16:50	0.018	3.81	K4.5 III	3750	5.1	23.	11
93813	Nu Hya	10:49	-16:11	0.028	3.11	K2 III	4300	4.7	22.	12
98262	54Nu Uma	11:18	+33:05	0.020	3.48	K3 III	4000	4.9	22.	12
98430	12Del Crt	11:19	-14:46	0.024	3.56	G8 III	4700	3.4	13.	36
99998	87 Leo	11:30	-03:00	0.015	4.77	K3.5 III	3600	4.0	13.	36
129078	Alp Aps	14:47	-79:02	0.029	3.83	K3 III	4000	4.3	18.	19
129456		14:43	-35:10	0.014	4.05	K3 III	4000	4.57	19.	17
129989	36Eps Boo	14:44	+27:04	0.016	2.70	K0 III	4500	4.4	21.	14
139063	39Ups Lib	15:37	-28:08	0.049	3.58	K3 III	4000	4.5	19.	17
139663	42 Lib	15:40	-23:49	0.049	4.96	K3 III	4000	2.4	5.4	206
140573	24Alp Ser	15:44	+06:25	0.053	2.65	K2 III	4300	5.2	27.	8.2
150798	Alp TrA	16:48	-69:01	0.031	1.92	K2 III	4300	11.6	134.	0.3
152786	Zet Ara	16:58	-55:59	0.044	3.13	K3 III	4000	7.6	53.	2.1
152980	Eps1 Ara	16:59	-53:09	0.005	4.06	K4 III	3900	4.0	15.	27
157244	Bet Ara	17:25	-55:31	0.034	2.85	K3 II	3700	6.2	33.	5.5
161096	60Bet Oph	17:43	+04:34	0.033	2.77	K2 III	4300	4.9	24.	10.4
163376		17:57	-41:42	-0.005	4.88	M0 III	3200	4.2	13.	36
167818		18:18	-27:02	0.033	4.65	K3 II	3800	4.1	15.	27
168454	19Del Sgr	18:20	-29:49	0.047	2.70	K3 III	4000	6.8	42.	3.4
169916	22Lam Sgr	18:27	-25:25	0.053	2.81	K1 III	4400	4.2	18.	19
173764	Bet Sct	18:47	-04:44	0.019	4.22	G4 II	5000	2.4	6.7	134
175575	37Xi 2Sgr	18:57	-21:06	0.011	3.51	K1 III	4400	3.7	14.	31
192876	5Alp1Cap	20:17	-12:30	0.007	4.24	G3 I	5300	2.0	6.0	167
197989	53Eps Cyg	20:46	+33:58	0.057	2.46	K0 III	4500	4.5	21.	14
204867	22Bet Aqr	21:31	-05:34	0.006	2.91	G0 I	5700	2.8	10.	60
219215	90Phi Aqr	23:14	-06:02	0.010	4.22	M1.5 III	3050	5.5	11.	50

\dagger Required integration time to achieve SNR=20 assuming rms sensitivity of $0.50*[t(min)]^{-1/2}$ mJy.

Table 2. A list of 39 bright giant and supergiant stars visible from Chajnantor that are non-variable and non-binary. These are selected from all giant and supergiant stars in the Bright Star Catalog with visible magnitude less than 5. The 650 GHz fluxes are computed assuming thermal emission from a star of given effective temperature (Allen 1973) with given estimated or measured diameter (Ochsenbein & Halbwegs 1982). These stars are brighter than the main sequence stars listed in Table 1 primarily because of their larger sizes.

Table 3: Estimated atmospheric phase fluctuations at the Chajnantor site.

Fraction of time	σ_θ at 11.2 GHz	ν at which $\sigma_\theta = 30^\circ$	ν at which $\sigma_\theta = 70^\circ$
0.75	2.95°	113 GHz	266 GHz
0.50	1.61°	209 GHz	487 GHz
0.25	0.93°	361 GHz	843 GHz
0.10	0.66°	509 GHz	1190 GHz

Table 3. Estimate of the fraction of time when the atmospheric phase rms error are less than 30 and 70° (13% and 50% loss due to de-correlation) at the Chajnantor site (from Holdaway & Owen 1995). Active phase correction may increase the maximum frequency quoted in this table by a factor of 3 to 4.

REFERENCES

- Allen, C. W. 1973, "Astrophysical Quantities," Third Edition (Athlone Press: London & Dover, NH), p.206
- Altenhoff, W. J., Johnston, K. J., Stumpff, P., & Webster, W. J. 1994, "Millimeter-wavelength Observations of Minor Planets," *A&A*, 287, 641
- Altenhoff, W. J., Baars, J. W. M., Schraml, J. B., Stumpff, P., & von Kappherr, A. 1996, "Precise Flux Density Determination of 1 Ceres with the Heinrich-Hertz-Telescope at 250 GHz," *A&A*, 309, 953
- Bock, D., Welch, J., Fleming, M., & Thornton, D. 1998, "Radiometer Calibration at the Cassagrain Secondary Mirror," in preparation
- Carilli, C. L., Lay, O., & Sutton, E. C. 1998, "Radiometric Phase Correction", MMA Memo in preparation
- Cornwell, T., & Fomalont, E. B. 1989, "Self-Calibration," in *Synthesis Imaging in Radio Astronomy*, eds. R. A. Perley, F. R. Schwab, & A. H. Bridle, ASP Conf. Series Vol. 6, p.185
- Holdaway, M. 1996, "Flux Calibration of the MMA," MMA Memo No. 149
- Holdaway, M. A. 1997a, "Sensitivity Comparisons of the Various LSA/MMA Collaboration Options," MMA Memo No. 177
- Holdaway, M. 1997b, "Effects of Pointing Errors on Mosaic Images with 8m, 12m, and 15m Dishes," MMA Memo No. 178
- Holdaway, M. 1998a, "Amplitude Fluctuations in Millimeter and Submillimeter Observations," in preparation
- Holdaway, M. 1998b, "Hour Angle Ranges for Configuration OPTimization," MMA Memo No. 201
- Holdaway, M., & Owen, F. 1995, "Correcting for Decorrelation Due to Atmospheric Phase Errors," MMA Memo 136
- Kutner, M. L., & Ulich, B. L. 1981, "Recommendations for Calibration of Millimeter-wavelength Spectral Line Data," *ApJ*, 250, 341
- Muhleman, D. O., & Berge, G. L. 1991, "Observations of Mars, Uranus, Neptune, Io, Europa, Ganymede, and Callisto at a Wavelength of

2.66 mm,” ICARUS, 92, 263

Ochsenbein, F. & Halbwachs, J. L. 1982, “A List of Stars with Large Expected Angular Diameters,” A&AS, 47, 523.

Perley, R. A. 1989, “High Dynamic Range Imaging,” in *Synthesis Imaging in Radio Astronomy*, eds. R. A. Perley, F. R. Schwab, & A. H. Bridle, ASP Conf. Series Vol. 6, p.287

Rupen, M. P. 1997, “The Astronomical Case for Short Integration Times on the Millimeter Array,” MMA Memo No. 192

Sandell, G. 1994, “Secondary calibrators at submillimeter wavelengths,” MNRAS, 271, 75

Ulich, B. L. 1974, “Absolute Brightness Temperature Measurements at 2.1-mm Wavelength,” ICARUS, 21, 254

Ulich, B. L., Davis, J. H., Rhodes, P. J., & Hollis, J. M. 1980, “Absolute Brightness Temperature Measurements at 3.5-mm Wavelength,” IEEE Trans. on Antennas Propag., Ap-28, 367